Supporting Information

Electrically Tunable Soft-Solid Block Copolymer Structural Color

Tae Joon Park,[†] Sun Kak Hwang,[†] Sungmin Park,[‡] Sung Hwan Cho,[†] Tae Hyun Park,[†] Beomjin Jeong,[†] Han Sol Kang,[†] Du Yeol Ryu,[‡] June Huh,[§] Edwin L. Thomas [#] and Cheolmin Park[†,]*

[†]Department of Materials Science and Engineering, Yonsei University, 50 Yonsei-ro, Seodaemun-gu, Seoul, 120-749 (Republic of Korea)

[‡]Department of Chemical and Biomolecular Engineering, Yonsei University, 50 Yonsei-ro, Seodaemun-gu, Seoul 120-749, Republic of Korea

[§]Department of Chemical and Biological Engineering, Korea University, Anam-dong, Seongbuk-gu, Seoul 136-713, Korea

[#]Department of Materials Science and Nano Engineering, Rice University, Houston, TX , 77005 , USA

*Corresponding author, E-mail cmpark@yonsei.ac.kr.

Phone numbers to Cheolmin Park

Office phone: +82-2-2123-2833

Fax:+82-2-312-5375

Supporting experiments

Binding energy calculation: The quantum mechanical computations for the optimized geometries and the binding energies of the model system, PS-Li^+TFSI^-, P2VP-Li^+TFSI^-, and QP2VP-Li^+TFSI^-, were performed using DFT method as implemented in Gaussian 09 program[1] with B3LYP functional[2] and 6-31* Gaussian basis set. In the model systems, only monomeric units of polymer species (Q2VP, 2VP) were considered for the sake of computational efficiency. The binding energies were obtained by the energy difference between the complex form and the isolated species.

Reflectance simulation: The FDTD method[3] is used to compute the reflectance of BCP layers by numerically solving Maxwell's equation[4] for the electric and magnetic fields in the mesh cells modeled for BCP PC layer with the perfectly matched layer[5] as a free space boundary condition. The BCP lamellae consisting 17 A-B bilayers is assumed to be strongly segregated and the refractive indices of A domain (n_A) and B domain (n_B) are given by $n_A = 1.59$ and $n_B = [n_{B,o}^2/\alpha_B + n_W^2(1-/\alpha_B)]^{1/2}$ with $n_{B,o} = 1.62$ and $n_W = 1.33$ where α_B is the swelling ratio of B domain capable of water adsorption.

Water sorption simulation and NPT MD simulation: Water sorption simulations for model sorbent systems (P2VP, P2VP/Li^+TFSI^- and QP2VP/Li^+TFSI^-) at fixed temperature and pressure (25 ^oC, 1 bar (fugacity of water = 4.95 kPa)) were performed using Grand Canonical Monte Carlo (GCMC) method with Metropolis sampling and COMPASS force field[6] (COMPASS II) as implemented in Sorption module of Material Studio package.[7] For the sorption trial moves to the model sorbent systems, the equilibration steps and the production steps were set to 10^5 and 5×10^6 Monte Carlo moves. Each model sorbent system was generated to consist of n chains (n=10 for P2VP, n=4 for P2VP/Li^+TFSI^- and QP2VP/Li^+TFSI^-) each with 10 monomeric units and the weight fractions of Li^+TFSI^- for P2VP/Li^+TFSI^- and QP2VP/Li^+TFSI^- were set to be 0.5, which were equilibrated by NPT molecular dynamics (MD) simulation at 25 ^oC and 1 bar for 1 ns using Forcite module of Material Studio. The same NPT MD simulation methods were employed for the computation of the pair correlation functions in the QP2VP/Li^+TFSI^-/water system where the fraction of water was given according to the water

sorption simulation. For all NPT MD runs, the electrostatic potential energy was calculated by the Ewald summation and the van der Waals potential energy was calculated by the atom based technique with a cutoff distance of 12.5 Å and a spline width of 1 Å. Nose-Hoover thermostat[8,9] and Berendsen barostat[10] were used for maintaining temperature (25 ^{o}C) and the pressure (1 bar) with the time step of 1 fs.

1. Frisch, M. J.; Trucks, G. W.; Schlegel, H. B.; Scuseria, G. E.; Robb, M. A.; Cheeseman, J. R.; Scalmani, G.; Barone, V.; Mennucci, B.; Petersson, G. A.; *et al.* GAUSSIAN 09 (Revision D.01), Gaussian, Inc., Wallingford CT, 2004.

2. Becke, A. D. Density-Functional Thermochemistry. III. The Role of Exact Exchange. *J. Chem. Phys*. **1993**, *98*, 5648-5652.

3. Yee, K. S. Numerical Solution of Initial Boundary Value Problems Involving Maxwell's Equations in Isotropic Media. *IEEE Trans. Antennas Prop.* **1966**, *14*, 302-307.

4. Maxwell, J. C. A Dynamical Theory of The Electromagnetic Field. *Philos. Trans. R. Soc. London* **1865**, *155*, 459-512.

5. Berenger, J.-P. J. A Perfectly Matched Layer for The Absorption of Electromagnetic Waves. *Comput. Phys*. **1994**, *114*, 185-200.

6. Sun, H. An ab Initio Force-Field Optimized for Condensed-Phase Applications Overview with Details on Alkane and Benzene Compounds. *J. Phys. Chem. B*, **1998**, *102*, 7338-7364.

7. Akkermans, R. L. C.; Spenley, N. A.; Robertson, S. H. Monte Carlo Methods in Materials Studio. *Mol. Simulat.* **2013**, *39*, 1153-1164.

8. Nose, S.; Klein, M. L. Constant Pressure Molecular Dynamics for Molecular Systems. *Mol. Phys.*

1983, *50*, 1055-1076.

9. Hoover, W. G. Canonical Dynamics: Equilibrium Phase-Space Distributions. *Phys. Rev. A* **1985**, *31*, 1695-1697.

10. Berendsen, H. J. C.; Postma, J. P. M.; Funsteren, W. F. Molecular Dynamics with Coupling to An External Bath. *J. Chem. Phys*. **1984**, *81*, 3684-3690.

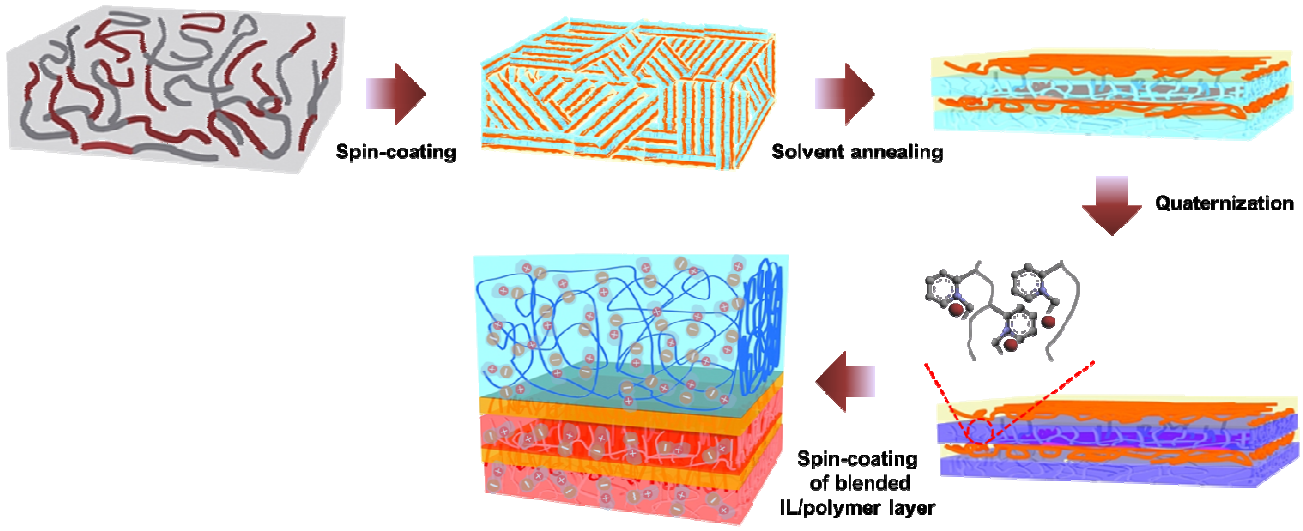

Figure S1. Schematic illustration for preparation of bi-layered BCP SC films.

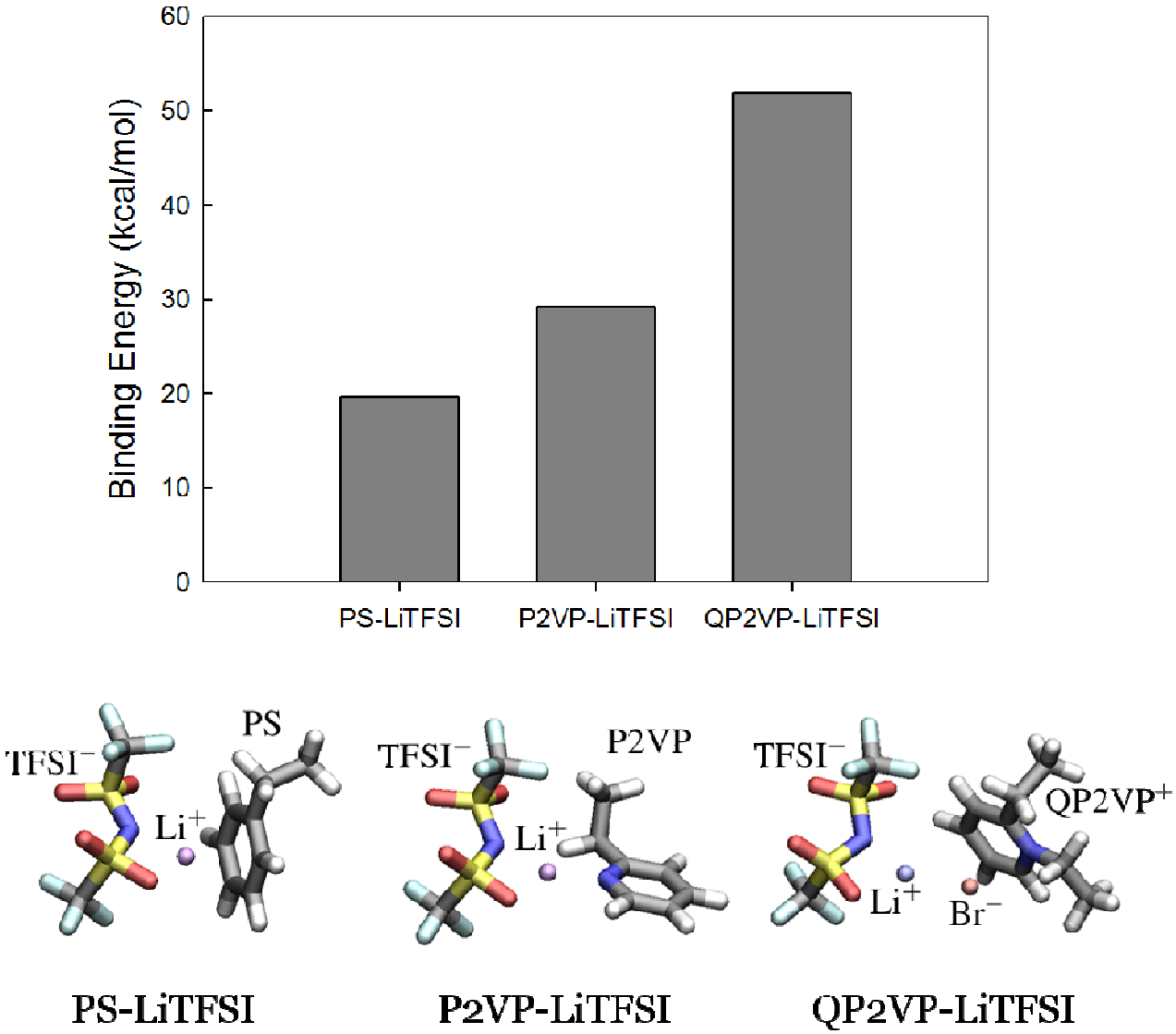

Figure S2. The binding energies and the optimized geometries of PS- LiTFSI, P2VP- LiTFSI, and QP2VP- LiTFSI, computed by DFT method with B3LYP functional and 6-31* Gaussian basis set.

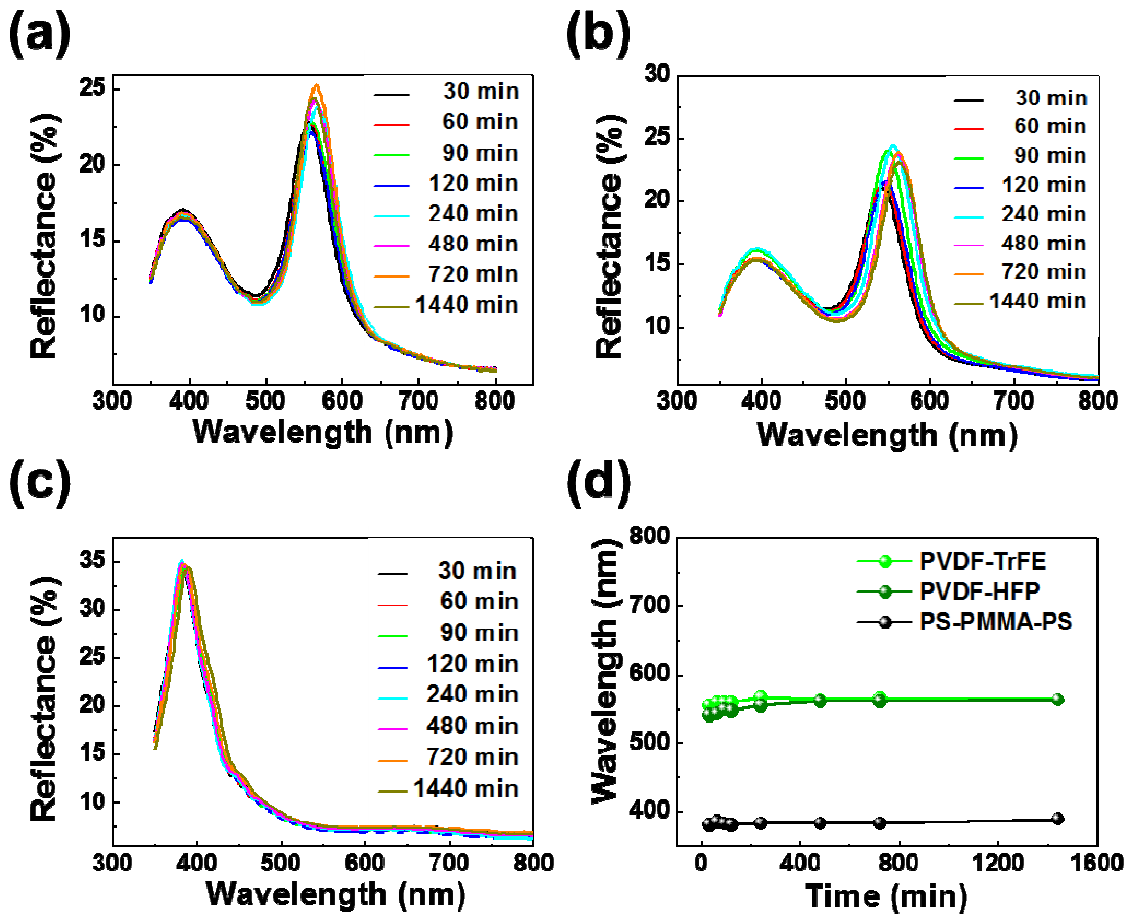

Figure S3. UV-vis spectra of the bi-layered BCP SC film with different polymer matrix: (a) PVDF-TrFE, (b) PVDF-HFP and (c) PS-PMMA-PS as a function of the time. (d) The bragg diffraction peak positions of bi-layered BCP SC films as a function of the time.

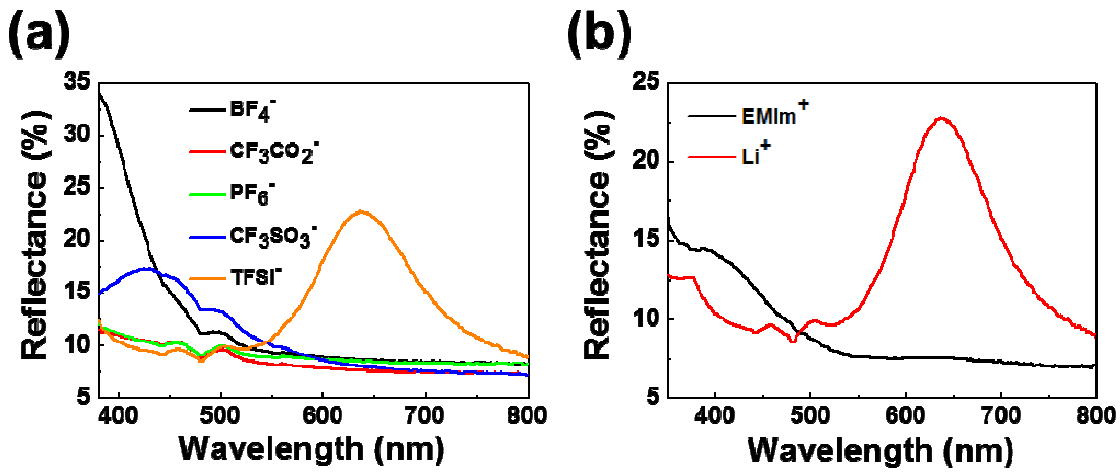

Figure S4. UV-vis spectra of the bi-layered BCP SC film (a) with different anion species such as BF_4^-, $CF_3CO_2^-$, PF_6^-, $CF_3SO_3^-$, $TFSI^-$. (Counter ion was Li^+) (b) with different cation species such as $EMIm^+$, Li^+. (Counter ion was $TFSI^-$)

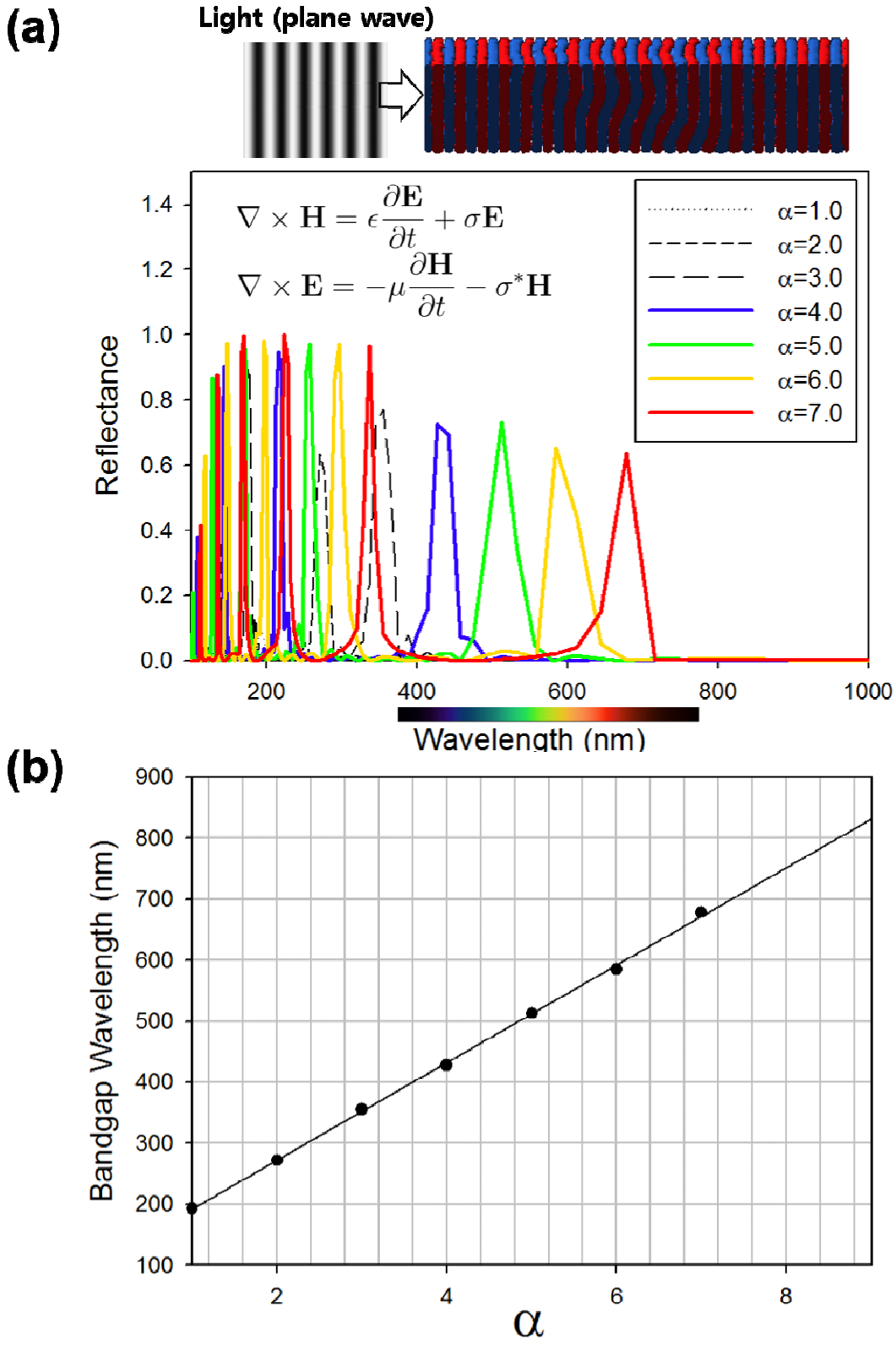

Figure S5. FDTD simulation in the case of plane wave passing though the BCP SC film. (a) UV-vis reflectance spectra with different swelling ratio α (b) A plot of bandgap wavelength as a function of α.

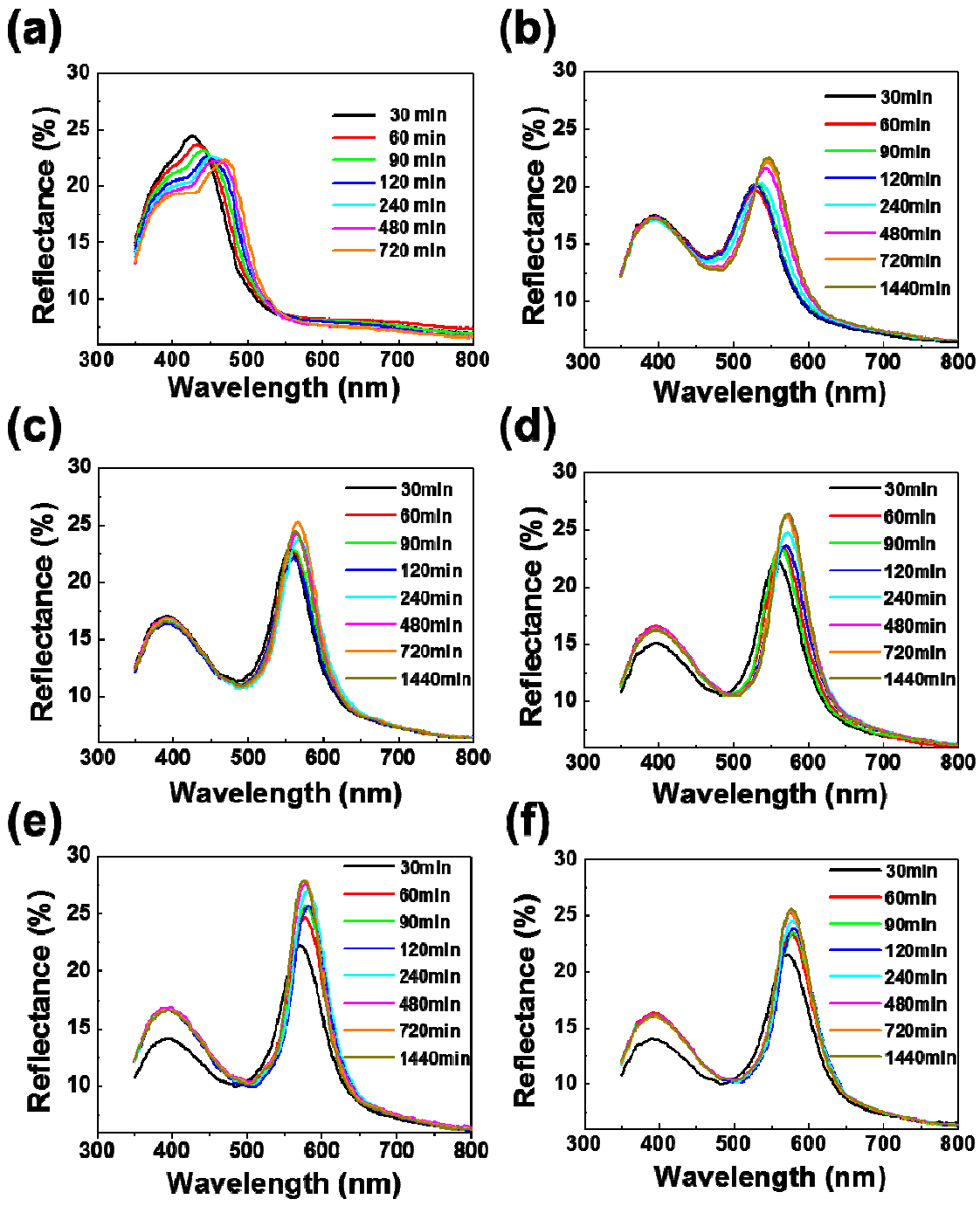

Figure S6. UV-vis reflectance spectra of the bi-layered BCP SC film with different IL concentration: (a) 200 wt%, (b) 300 wt%, (c) 500 wt%, (d) 700 wt%, (e) 1000 wt% and (f) 1200wt%. Blended IL/Polymer layer comprised of LiTFSI and PVDF-TrFE.

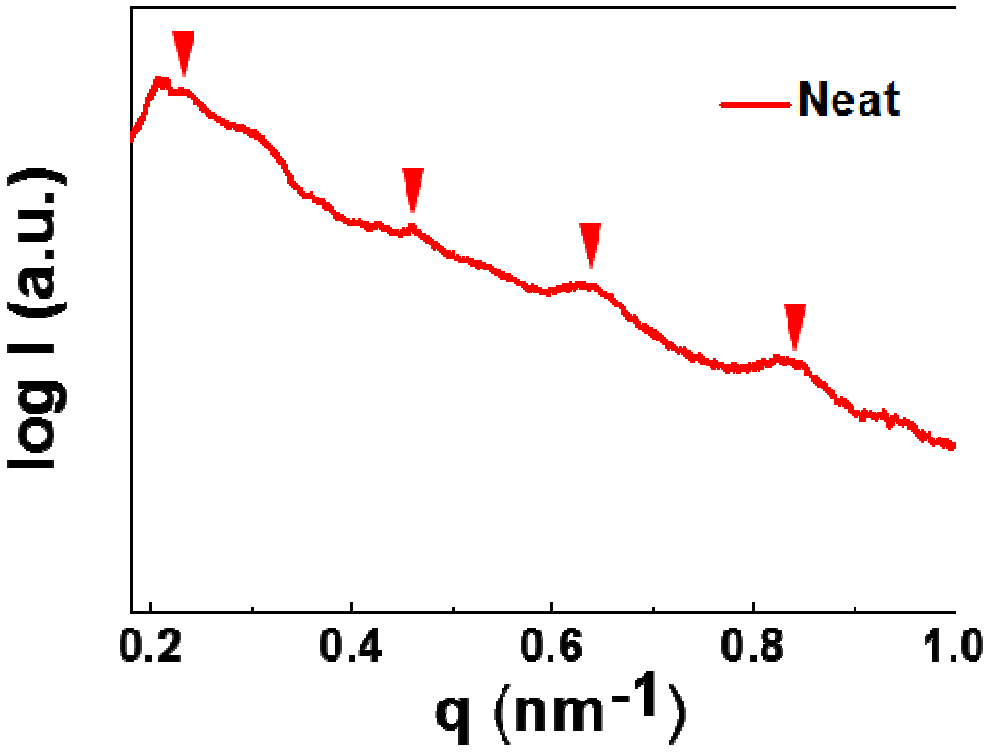

Figure S7. GISAXS profiles of the neat BCP SC films. The scattering vector q_1 appeared at 0.2278 nm^{-1}.

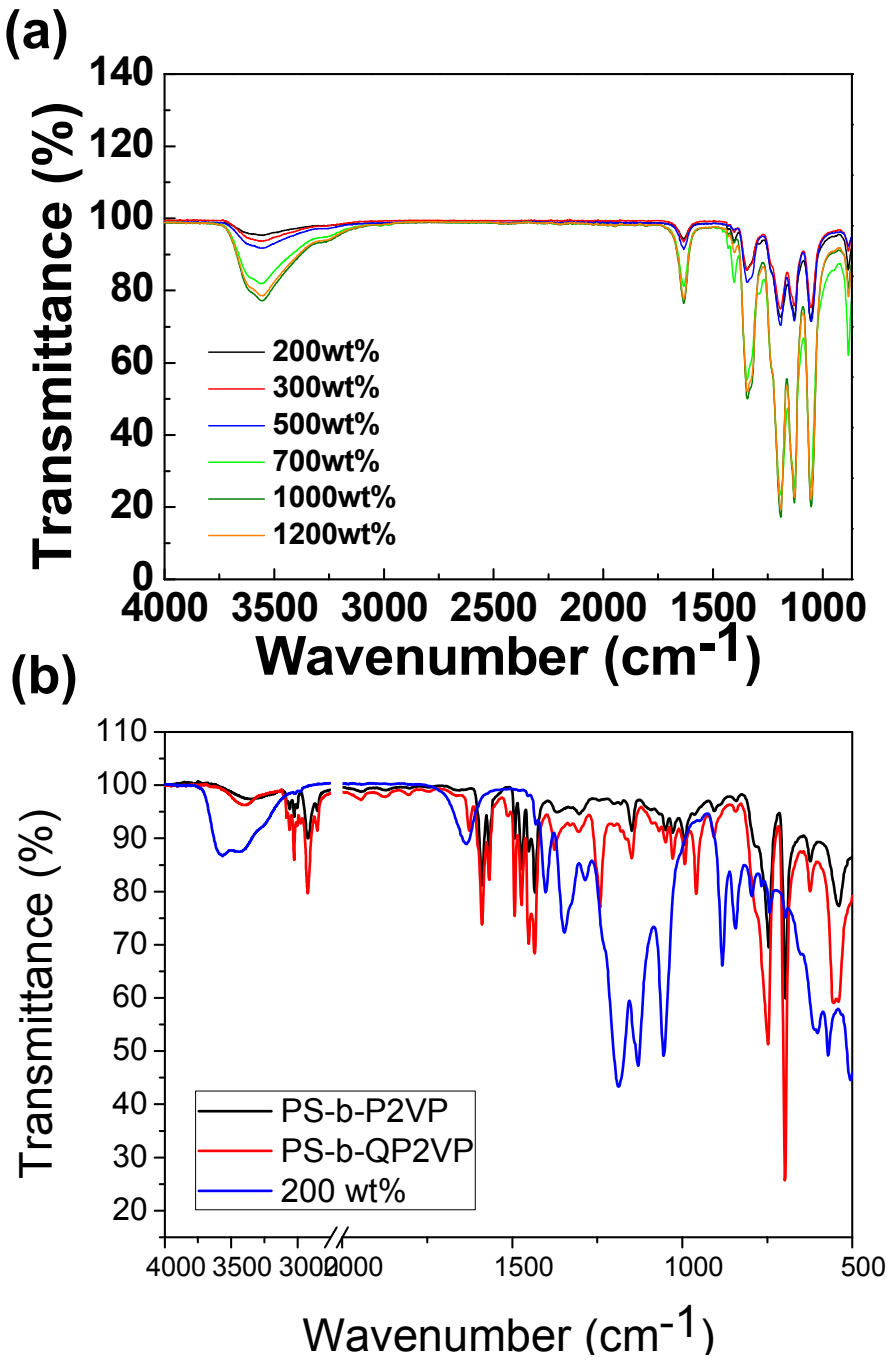

Figure S8. (a) FT-IR spectra of bi-layered BCP SC films as a function of IL concentration. As IL concentration increases, Transmittance decreases at 3500 ~ 3600 cm^{-1} arising from the vibration of hydroxyl group in water molecule. (b) FT-IR spectra of a PS-*b*-P2VP and a PS-*b*-QP2VP film. A spectrum of bi-layered BCP SC film with 200 wt% IL-polymer layer is shown for comparison.

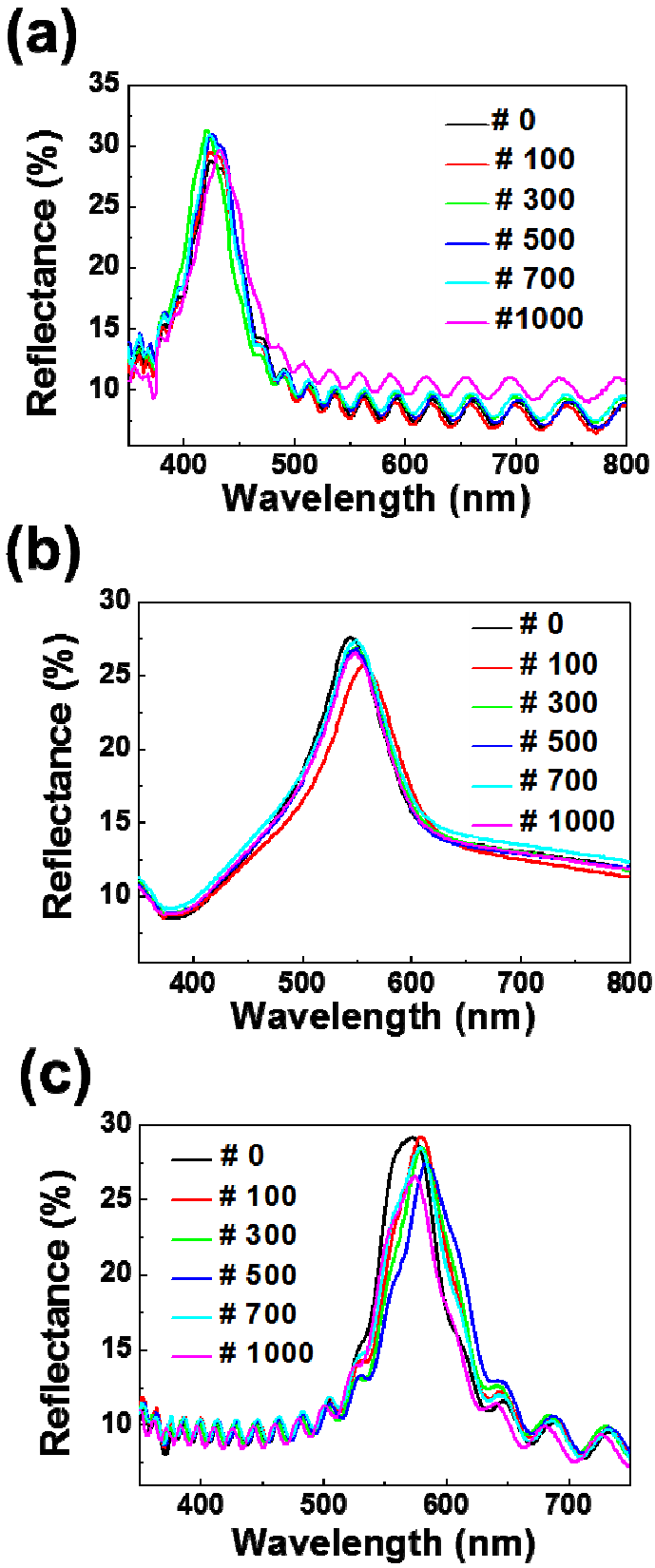

Figure S9. UV-vis reflectance spectra of the bi-layered BCP SC films prepared on poly(ethylene terephthalate) substrates with different IL concentration: (a) 200wt%, (b) 300wt%, and (c) 1200wt% as a function of the number of bending.

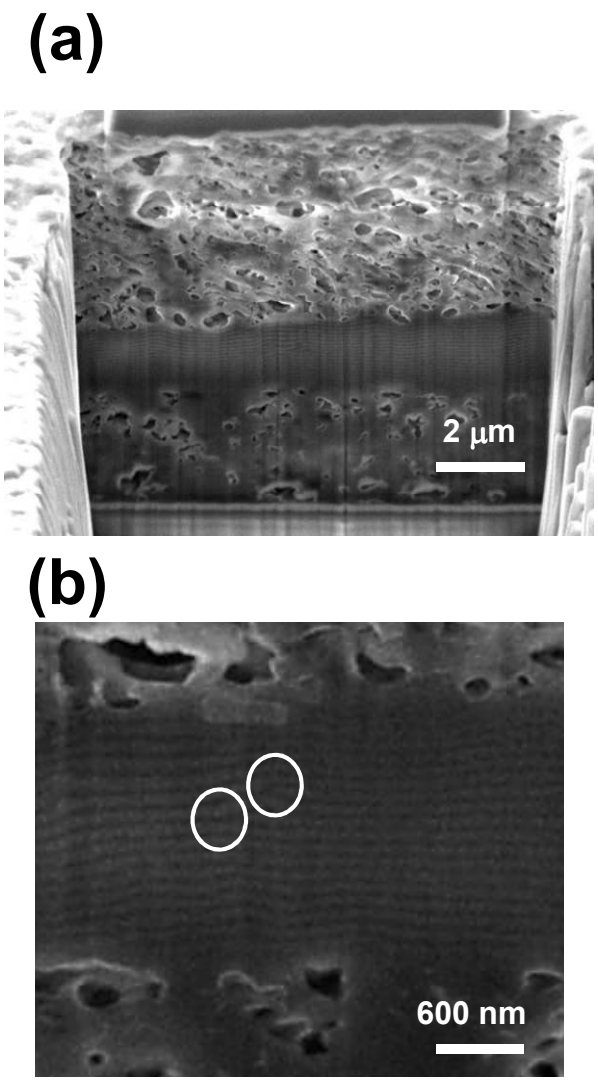

Figure S10. (a and b) Cross-sectional SEM images of a switchable solid-type BCP SC device. The device was directly milled by focused ion beam. (b) A magnified image of the BCP layer with dislocations highlighted by circles.

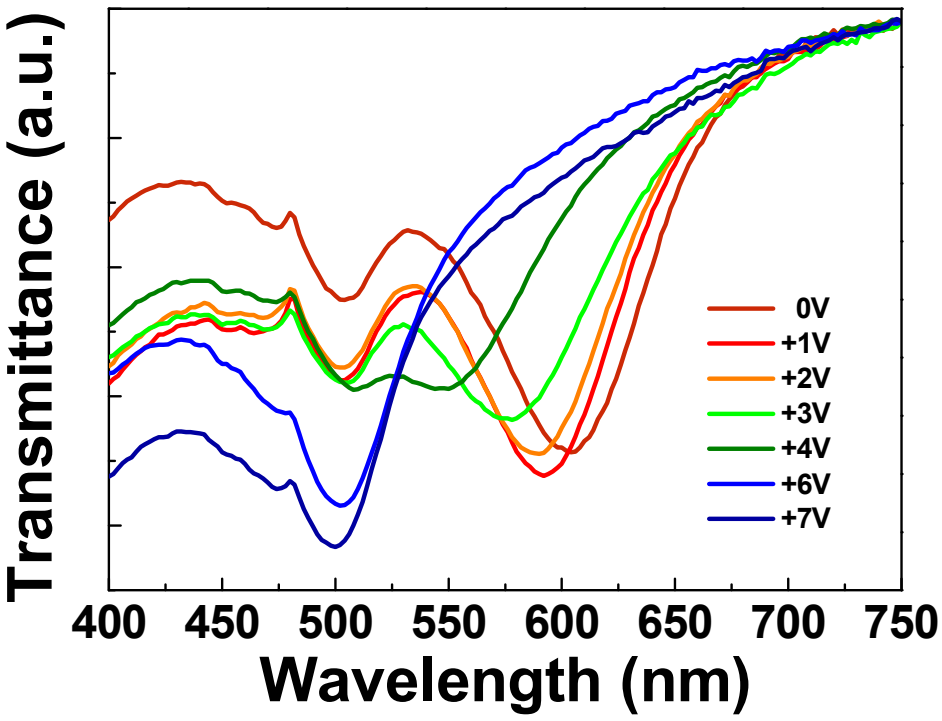

Figure S11. UV-vis reflectance spectra of the switchable solid-type BCP SC device as a function of applied voltage.

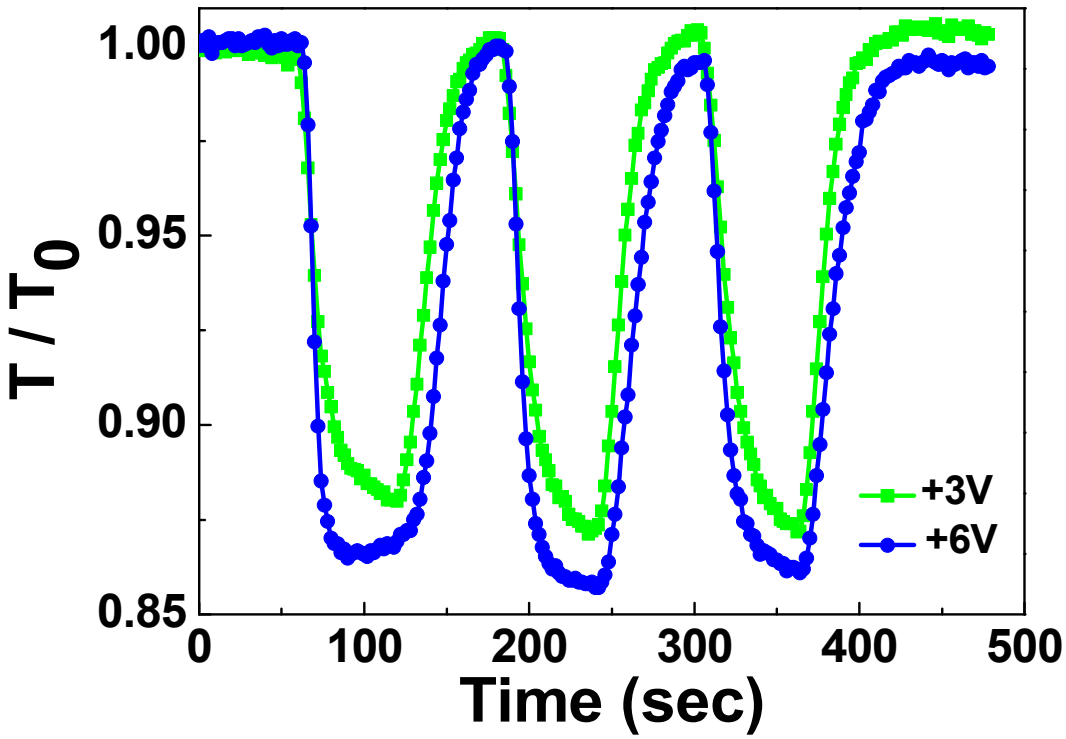

Figure S12. Switching properties of a capacitor type SC device with different applied voltages during the 3 cycles.